2014

Residential solar air conditioning: Energy and Exergy analyses of an ammonia-water absorption cooling system

Julia Aman
University of Windsor

David S-K Ting
University of Windsor

Paul Henshaw
University of Windsor

Applied Thermal Engineering 62 (2014) 424–432

Contents lists available at ScienceDirect

Applied Thermal Engineering

journal homepage: www.elsevier.com/locate/apthermeng

Residential solar air conditioning: Energy and exergy analyses of an ammonia–water absorption cooling system

J. Aman*, D.S.-K. Ting, P. Henshaw

Turbulence and Energy Laboratory, Centre for Engineering Innovation, University of Windsor, 401 Sunset Avenue, Windsor, Ontario N9B 3P4, Canada

HIGHLIGHTS

- 10 kW solar thermal driven ammonia–water air cooled absorption chiller is investigated.
- Energy and exergy analyses have been done to enhance the thermal performance.
- Low driving temperature heat sources have been optimized.
- The efficiencies of the major components have been evaluated.

ARTICLE INFO

Article history:
Received 14 June 2013
Accepted 4 October 2013
Available online 12 October 2013

Keywords:
Absorption
Air-conditioning
Solar thermal
COP
Exergy losses
Exergetic efficiency

ABSTRACT

Large scale heat-driven absorption cooling systems are available in the marketplace for industrial applications but the concept of a solar driven absorption chiller for air-conditioning applications is relatively new. Absorption chillers have a lower efficiency than compression refrigeration systems, when used for small scale applications and this restrains the absorption cooling system from air conditioning applications in residential buildings. The potential of a solar driven ammonia–water absorption chiller for residential air conditioning application is discussed and analyzed in this paper. A thermodynamic model has been developed based on a 10 kW air cooled ammonia–water absorption chiller driven by solar thermal energy. Both energy and exergy analyses have been conducted to evaluate the performance of this residential scale cooling system. The analyses uncovered that the absorber is where the most exergy loss occurs (63%) followed by the generator (13%) and the condenser (11%). Furthermore, the exergy loss of the condenser and absorber greatly increase with temperature, the generator less so, and the exergy loss in the evaporator is the least sensitive to increasing temperature.

1. Introduction

According to the International Energy Agency, present energy supply and use are economically, environmentally and socially unsustainable [29]. The International Institute of Refrigeration reported that refrigeration and air conditioning systems consume approximately 15% of the total world electricity generation [27]. Also, 45% of the total residential energy consumption is due to air conditioning systems [10]. Approximately 80% of the world's electricity is being generated from fossil fuels that contribute significantly to greenhouse gas emissions [16]. This is predicted to increase with the rise in world summer temperature of 2–4 °C by the end of the century [22]. Climate change and an increase in the standard of living will also increase the demand for air-conditioning, which will further impose a significant increase in primary energy consumption. This is especially poignant in developing countries, where the rapid growth of economy and consequent prosperity has caused a rapid rise in conventional air conditioning system installation and use. The increase in electrical energy demand due to the population growth, increased demand for air-conditioning and expanding industries in these countries is exceeding the growth of available electrical power [20]. For example, according to India's Central Electricity Authority, India has a power shortfall of 8%, which peaks during the summer. This results in regular power outages in the summer, which can last a couple of hours [9]. On the other hand, the abundant amount of solar radiation in most developing countries is a renewable energy source, which is available most of the year [5]. This abundant solar power makes solar cooling technology a suitable alternative, particularly for people who live in the remote areas and suffer from a shortage of electricity.

The traditional vapor compression machine used for air-conditioning operates on electrically-driven compressor chillers.

* Corresponding author.
E-mail address: amanj@uwindsor.ca (J. Aman).

1359-4311/$ – see front matter © 2013 Elsevier Ltd. All rights reserved.
http://dx.doi.org/10.1016/j.applthermaleng.2013.10.006

Their operation causes a high energy demand during the peak load period in the summer, which triggers the start-up of fossil fuel power plants in jurisdictions, such as Ontario, where the base load is met by nuclear power. Therefore, it is crucial to reduce the consumption of unsustainable fossil fuels, and at the same time, it is imperative to promote sustainable energy technology to meet the increasing energy demand for cooling. Solar thermal technologies are a sustainable means to meet the increasing energy demand, and the highest solar radiation coincides with the peak cooling period in summer [19]. Accordingly, solar thermal cooling could reduce energy needs during the peak periods in summer by replacing electrically driven compressor chillers with thermally driven chillers. The cooling supply can be extended beyond sunset by incorporating heat storage into the system.

Currently, different cooling technologies driven by waste heat are available, but they are mostly sized for 50 kW capacities, whereas small scale (less than 10 kW) technology is still emerging and requires low-cost systems with minimal maintenance requirements. Recently, some companies have taken initiatives to improve absorption chillers in the power range from 50 kW down to 5 kW [27]. But very few chillers are available for small scale cooling applications and they are not optimized for solar thermal power applications [7]. According to the International Energy Agency, small-scale system design requires R&D effort in order to develop low-cost systems, integrate them with existing equipment and optimize operation in new developments [29]. Small-scale technology development should focus on compact machines with higher coefficients of performance (COPs) at low driving heat temperatures.

The most common method for producing thermally activated cooling is sorption cooling. Sorption includes both absorption and adsorption: "absorption is the process in which a substance in one phase is incorporated into another substance of a different phase (*e.g.* gas being absorbed by a liquid); whereas adsorption refers to the use of a solid for adhering or bonding ions and molecules of another substance onto its surface" [13]. In sorption cooling systems, thermal compression of the refrigerant is employed instead of mechanical compression. These two technologies are mostly used in central air conditioning systems with decentralized fan coils or cooled ceilings [37]. Furthermore, the absorption system with air cooling can also reduce the initial and maintenance cost associated with cooling towers [14]. The present work is devoted to provide air conditioning by an air-cooled absorption refrigeration system which is driven by solar energy and uses environmentally friendly refrigerants.

In an absorption cycle, a refrigerant and an absorbent are a pair of substances that work together. Lithium bromide–water and ammonia–water are the most common working pairs in refrigeration and air conditioning absorption refrigeration systems. With evaporation temperatures about 5–10 °C, the lithium bromide–water pair is widely used for air cooling applications; but when evaporation temperatures below 0 °C are required, the ammonia–water pair is mostly used, such as in small size air conditioning and large industrial applications [1]. The crystallization problem limits the lithium bromide–water solution to a narrow concentration and the absorber lower temperature to approximately 40 °C [13]. The high absorber temperature and high initial cost restrain the use of lithium bromide–water absorption chillers in residential scale applications. Moreover, the lithium bromide–water absorption chiller is difficult to be air cooled, because air cooling increases the risk of crystallization for this chiller [23]. Whereas, ammonia has low freezing point (−77.7 °C) which does not crystallize at low evaporating temperature and this helps the condenser and the absorber units of this chiller to cool with direct air cooling. In addition, ammonia is a high pressure refrigerant with a low specific volume which makes the water–ammonia chiller more compact. For residential buildings, the required cooling capacity should be within the range of 3–10 kW [39].

The direct fired water–ammonia chiller has been available for air conditioning since 1964 [31]. But due to the lower efficiency, the commercial availability of this chiller has been eliminated. In the last few years, however, a few water–ammonia chillers with high efficiency have been developed for residential and light commercial applications employing the GAX (generator–absorber exchanger) concept. In GAX absorption cycle, the efficiency is high because the difference of ammonia concentration in rich solution and weak solution is large [39]. The Robur Company (Italy) first introduced the GAX technology in a water–ammonia absorption chiller with a cooling capacity of 17.7 kW and a COP of 0.71 [21]. But the problem with the GAX cycle is that it only operates with a high driving temperature: 160 °C is needed to reach a COP of 0.75 and the COP increases to 1.0 when the driving temperature reaches nearly 200 °C [32]. For this reason, this kind of chiller was originally designed to use direct-fired gas.

Another commercial water–ammonia absorption system is SolarNext of Germany. They introduced a commercially available solar powered 10 kW single-effect water–ammonia absorption chiller for residential and commercial air conditioning applications that has a driving temperature of 85–78 °C, resulting in a 19–16 °C chilled water temperature with a COP of 0.63 [25]. This system also uses a cooling tower for absorber and condenser cooling.

Many prototypes have been built for ammonia–water absorption chillers but those are either not direct air cooled or not commercially available. Gazi University in Turkey built a prototype of a water–ammonia absorption heat pump operated by solar energy which has an optimum driving temperature of 80 °C for the best COP, and an evaporating temperature of 3 °C which means that it could be used for air conditioning and preservation of food [35]. The University of Madrid in Spain constructed a 2 kW prototype of a low-power water–ammonia absorption chiller driven by solar energy. This prototype used a transfer tank instead of a solution pump, which did not operate well, and the experimental COP was lower than 0.05 [12]. The University of Applied Sciences, Stuttgart in Germany built a 2.5 kW prototype solar powered ammonia–water diffusion absorption chiller which is driven by generator temperatures from 150 to 170 °C. For this system, the best cooling capacity reached was 1.5 kW, at COP values between 0.2 and 0.3 [24]. A 10 kW cooling capacity water–ammonia absorption chiller prototype was also developed at ITW Stuttgart in Germany. At driving temperature of 90 °C, cold water temperatures of 15 °C could be achieved with a cooling capacity of 7.2 kW and a COP of 0.66 [26]. The French National Institute for Solar Energy developed a 4.2 kW prototype water–ammonia absorption chiller operating at 80, 27 and 18 °C temperatures for the generator, absorber/condenser and evaporator, respectively. It achieved a COP of 0.65 [7].

In short, the lower efficiency of ammonia–water chillers compared with LiBr–H_2O chillers, limits their widespread use for residential and light-commercial air conditioning applications. In this respect, research for the improvement of the thermal performance of the ammonia–water absorption cycle has been increased.

The potential of the ammonia–water absorption cycle for a small scale solar thermal air conditioning application has been investigated in this paper. In order to reduce the size and increase the thermal performance, this system is intended for air cooling instead of water cooling and a low temperature heat driving source like a flat plate solar collector is anticipated. The energy and exergy analyses of the model ammonia–water absorption cycle will identify the components of the system that have the greatest effect on the system thermal performance. The exergy losses of different components will determine the least efficient components of the system. In this study, the potential and the thermal performance of the system and its exergetic efficiency will be compared in different operating conditions.

2. Cycle operation principles

Solar thermal cooling systems usually consist of solar thermal collectors linked to a sorption chiller. The main components of such a system are: the solar collectors; a heat storage tank; the heat-driven cooling device; the indoor air cooling system and an auxiliary (backup) subsystem. The backup system may be an auxiliary heater connected in parallel to the collector. A single-effect ammonia–water absorption solar thermal cooling system is illustrated in Fig. 1, where water is the absorbent and ammonia is the refrigerant. The main four parts in a basic absorption cycle are: the generator, the condenser, the evaporator and the absorber. There are other 'auxiliary' components: rectifier, expansion valves, heat exchanger and pump.

In this system, as ammonia is the solute, the rich ammonia solution is heated in the generator by the solar collector and ammonia evaporates, leaving a hot weak solution in the generator [4]. From the generator, the high pressure ammonia vapor (State 1) is condensed to high pressure liquid ammonia (State 2) in the condenser; see Fig. 1. The condensed ammonia is then reduced in pressure while passing through the throttle valve (becoming State 3), and evaporates in the evaporator, where the cooling effect occurs. After leaving the evaporator (State 4), the low pressure ammonia vapor refrigerant enters the absorber, where it's absorbed by the cold weak solution in the absorber and becomes a rich solution of water saturated with ammonia. From the absorber, the rich solution is pumped to the generator (State 5–7) by the solution pump. The weak hot ammonia solution which was left in the generator after evaporation of the ammonia passes through the pressure reducing throttle valve and flows back to the absorber (State 8–10) at low pressure.

The ammonia–water cycle requires a rectifier to purify the ammonia because both water and ammonia are volatile. Without a rectifier, the ammonia vapor from the generator may contain some water vapor which could form ice in the condenser, block the throttling valve and perhaps freeze in the pipeline [30]. Also, water contaminant entering the evaporator would raise the evaporating temperature and lower the cooling effect of the evaporator [13]. A solution heat exchanger, as shown in Fig. 1, is normally added to the cycle in order to improve the cycle performance [2]. The solution heat exchanger is important for heat recovery, without which the

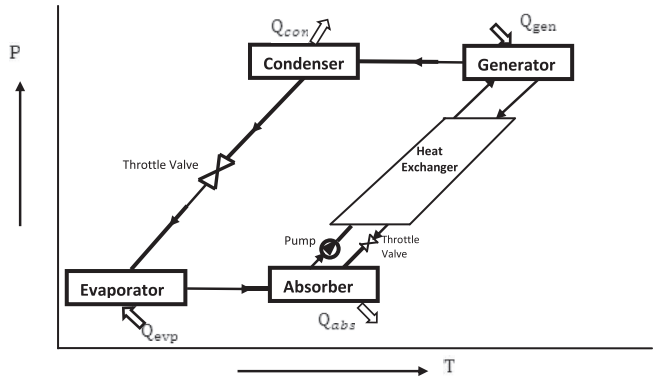

Fig. 2. Pressure, concentration and temperature diagram of ammonia–water mixture.

COP values of the cycle would be much lower [Sun [36]]. In the absorption refrigeration cycle, the pump is the only part which requires work input. However, this work is very small compared to that used by the compressor in a vapor compression cycle system [8].

Fig. 2 illustrates the heat flow pattern of the ammonia–water absorption cycle. The high temperature heat from the solar collector goes into the generator, and low temperature heat from the air conditioned area goes into the evaporator. The absorber and the condenser are the components that reject heat, at just above atmospheric temperature, to the environment.

The heat can be provided by flat plate, evacuated tube or concentrating solar collectors that are capable of delivering 70–120 °C fluid to the generator. A single effect ammonia–water absorption chiller can be driven by this generator temperature at a COP of 0.3–0.7 [39]. Due to the necessary rectification and lower vaporization heat of ammonia, as opposed to water, the COP of an ammonia–water cycle is lower than that of a lithium bromide–water cycle with the same cooling capacity [17]. Focusing on exergy destruction or irreversibility is a more direct way to analyze the potential for the improvement of the system performance. In this regard, energy and exergy analyses were performed in order to identify the locations of greatest exergy losses and the components with lower exergy loss in the process.

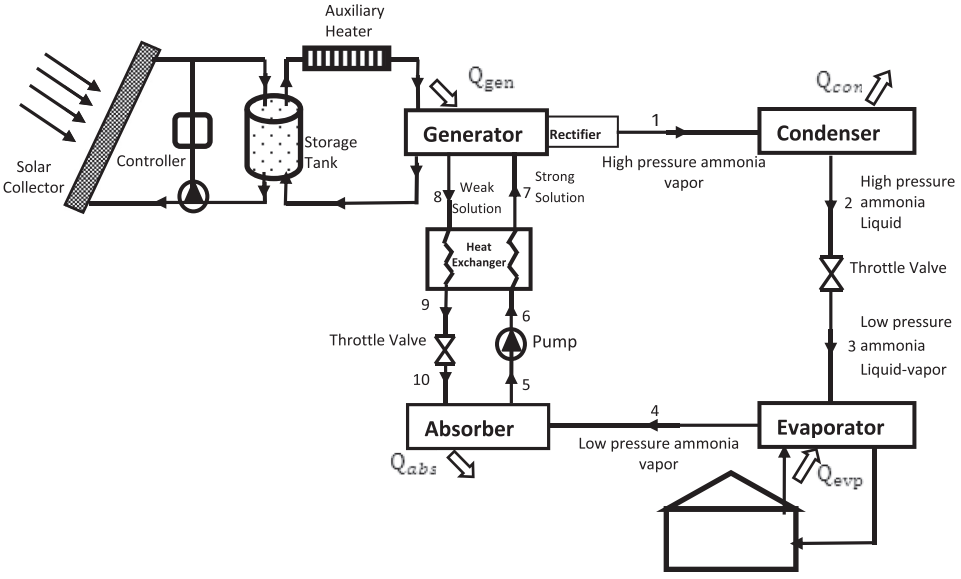

Fig. 1. Schematic diagram of the solar ammonia–water absorption cooling cycle.

3. Thermodynamic model

In analyzing this system, the principles of mass and energy conservation, and the second law of thermodynamics have been applied to each component. This study is limited to the steady flow steady state condition.

3.1. First law analysis (energy method)

In order to analyze the thermodynamic first law for the absorption system, the following principal equations are used to determine the mass and energy conservation at each component.

$$\text{Mass conservation}: \sum \dot{m}_{in} - \sum \dot{m}_{out} = 0 \quad (1)$$

$$\text{Energy conservation}: \sum \dot{Q} = \sum \dot{m}_{out} h_{out} - \sum \dot{m}_{in} h_{in} + \dot{W} \quad (2)$$

where $\dot{m}$ is the mass flow rate (kg/s), h is the specific enthalpy (kJ/kg) and $\dot{Q}$ is the heat transfer rate (kW). The amount of heat transfer to and from each component are determined by the heat balance over each component of the system. The heat transfer for generator, heat exchanger, pump, absorber, condenser and evaporator are represented by Equations (3)–(15).

For the generator, the mass and energy balances are:

$$\text{Total mass balance}: \dot{m}_7 = \dot{m}_1 + \dot{m}_8 \quad (3)$$

$$NH_3 \text{ mass balance}: X_7 \dot{m}_7 = \dot{m}_1 + X_8 \dot{m}_8 \quad (4)$$

where X is the NH_3 mass fraction in solution.

$$\text{Energy balance}: \dot{Q}_{gen} = \dot{m}_1 h_1 + \dot{m}_8 h_8 - \dot{m}_7 h_7 \quad (5)$$

The mass flow rate of the weak and strong solutions can be calculated from Equations (3) and (4),

$$\dot{m}_8 = \frac{1 - X_7}{X_7 - X_8} \dot{m}_1 \quad (6)$$

$$\dot{m}_7 = \frac{1 - X_8}{X_7 - X_8} \dot{m}_1 \quad (7)$$

The circulation ratio can be determined from Equation (8) which is the indication of required pumping power. It can be defined as the ratio of the mass flow rate of the strong solution going into the generator and the mass flow rate of the refrigerant [18].

$$CR = \frac{\dot{m}_7}{\dot{m}_1} \quad (8)$$

Equations (9) and (10) represent the energy balance for the solution heat exchanger.

$$T_9 = \eta_{HEX} T_6 + (1 - \eta_{HEX}) T_8 \quad (9)$$

where η_{HEx} is the heat exchanger efficiency.

$$h_7 = h_6 + \frac{\dot{m}_8}{\dot{m}_6} (h_8 - h_9) \quad (10)$$

The energy increase by pumping is

$$h_6 = h_5 + (P_6 - P_5) v_6 \quad (11)$$

$$\dot{W}_p = (P_6 - P_5) v_6 \quad (12)$$

Energy balances for the condenser, evaporator and absorber yield:

$$\text{Energy balance for condenser}: \dot{Q}_{cond} = \dot{m}_1 (h_1 - h_2) \quad (13)$$

$$\text{Energy balance for evaporator}: \dot{Q}_{eva} = \dot{m}_1 (h_4 - h_3) \quad (14)$$

$$\text{Energy balance for absorber}: \dot{Q}_{abs} = \dot{m}_4 h_4 + \dot{m}_{10} h_{10} - \dot{m}_5 h_5 \quad (15)$$

The coefficient of performance (COP) is the ratio of the useful energy gained from the evaporator to the primary energy supply to the generator and mechanical work done by the pump of the system [34].

$$COP = \frac{\text{useful energy output}}{\text{primary energy input} + \text{work done by pump}} = \frac{\dot{Q}_{eva}}{\dot{Q}_{gen} + \dot{W}_p} \quad (16)$$

3.2. Second law analysis (exergy method)

Exergy "is defined as the maximum amount of work potential of a material or an energy stream, in relation to the surrounding environment" [33]. The exergy balance in a control volume during a steady state process is stated as [34]:

$$\dot{E}_{D,i} = \sum (\dot{m}e)_{in} - \sum (\dot{m}e)_{out} + \sum \dot{Q} \left(1 - \frac{T_o}{T}\right)_{in} - \sum \dot{Q} \left(1 - \frac{T_o}{T}\right)_{out} + \sum \dot{W} \quad (17)$$

where $\dot{E}_{D,i}$ represents the rate of exergy loss (destruction) of each component in the system. On the right hand side of the equation, the first two terms represent the amount of the exergy entering and leaving the steady flow process in terms of mass transfer. The third and fourth terms are the exergy loss in terms of heat transfer, Q, to/from bodies maintained at constant temperature, T. The last term is the mechanical work transfer to or from the control volume. The exergy is expressed in terms of four types: physical, kinetic, potential and chemical exergy. Kinetic and potential exergy are assumed to be neglected and the chemical exergy is set to zero because there is no loss or gain of chemical substances from the cycle to the environment [38], so the exergy per unit mass of a fluid stream can be defined as [40]:

$$e = (h - h_o) - T_o (s - s_o) \quad (18)$$

where e is the specific exergy, h and s are the enthalpy and entropy of the fluid at temperature T, whereas, h_o and s_o are the enthalpy and entropy of the fluid at environmental temperature T_o. In this analysis, T_o was set to 298.15 K. In a process, the principle exergy losses are due to heat transfer under a temperature difference with the surrounding and unrestricted expansion [34]. The reference enthalpy and entropy of the rich NH_3–H_2O solution is considered at reference pressure, $P_0 = 101.325$ kPa and is assumed to have a NH_3 concentration equal to 55.05%.

The exergy loss in each component and the total exergy loss for the system can be written as:

$$\dot{E}_{D,gen} = \dot{m}_7 e_7 - \dot{m}_8 e_8 - \dot{m}_1 e_1 + Q_{gen} \left(1 - \frac{T_o}{T_{gen}}\right) \quad (19)$$

$$\dot{E}_{D,con} = \dot{m}_1 (e_1 - e_2) - Q_{con} \left(1 - \frac{T_o}{T_{con}}\right) \quad (20)$$

$$\dot{E}_{D,\text{eva}} = \dot{m}_1(e_3 - e_4) + Q_{\text{eva}}\left(1 - \frac{T_o}{T_{\text{eva}}}\right) \quad (21)$$

$$\dot{E}_{D,\text{abs}} = \dot{m}_4 e_4 + \dot{m}_{10} e_{10} - \dot{m}_5 e_5 - Q_{\text{abs}}\left(1 - \frac{T_o}{T_{\text{abs}}}\right) \quad (22)$$

$$\dot{E}_{D,\text{total}} = \dot{E}_{D,\text{gen}} + \dot{E}_{D,\text{con}} + \dot{E}_{D,\text{eva}} + \dot{E}_{D,\text{abs}} \quad (23)$$

A non-dimensional exergy loss of each component can be defined as the ratio of the exergy loss in each component to the total exergy loss of the system [40]. And it is written as follows for each component:

$$\text{Non} - \text{dimentional exergy loss} = \frac{\dot{E}_{D,i}}{\dot{E}_{D,\text{total}}} \quad (24)$$

The maximum thermal performance of an absorption refrigeration system is determined by assuming that the entire cycle is totally reversible (*i.e.*, the cycle involves no irreversibilities nor any heat transfer through a differential temperature difference) [8], in which case the overall maximum thermal performance of an absorption refrigeration system under reversible condition becomes:

$$\text{COP}_E = \left(1 - \frac{T_o}{T_{\text{gen}}}\right)\left(\frac{T_{\text{eva}}}{T_0 - T_{\text{eva}}}\right) \quad (25)$$

The second law efficiency of the absorption system leads to computing the exergetic efficiency, which is defined as the ratio of the useful exergy gained from a system to that supplied to the system [15]. The exergetic efficiency can be determined by the ratio of actual coefficient of performance (COP) to the maximum possible coefficient of performance (reversible COP), under the same operating conditions:

$$\eta_{\text{ex}} = \frac{\text{COP}}{\text{COP}_E} \quad (26)$$

3.3. Thermodynamic properties

In Fig. 1, States (1)–(4) require the thermodynamic properties for NH_3 and States (5)–(10) are based on NH_3–H_2O mixtures. The two phase equilibrium pressure and temperature of NH_3, the specific enthalpies of saturated NH_3 liquid and NH_3 vapor in terms of temperature, the relation between saturation equilibrium pressure, concentration and temperature of an ammonia–water mixture and the specific volume of the mixture have been calculated using equations from Ref. [36]. The entropy of an ammonia–water mixture in the saturated liquid phase in terms of temperature, and concentration has been calculated by using a correlation from Ref. [3].

3.4. Theoretical considerations

In this analysis, the following assumptions have been considered:

1. The system is operating under steady state conditions.
2. Ammonia–water solutions are presumed to be in equilibrium in the generator and in the absorber at their respective pressures and temperatures.
3. Unintentional pressure drops and heat losses in the pipelines and system components are negligible. So heat transfer to and from the surroundings is negligible, other than at the generator, condenser, evaporator and absorber.
4. All throttle valves are under adiabatic condition, which results in constant enthalpy processes.
5. The circulating pump is isentropic.
6. The vapor leaving the generator/rectifier is 100% ammonia.
7. The refrigerant states leaving the condenser and evaporator are saturated liquid and saturated vapor.
8. The ammonia–water solution at the absorber outlet is a rich solution at the absorber temperature, respectively.
9. The condenser and the absorber are air cooled at atmospheric temperature 25 °C.

4. Results and analysis

By analyzing the thermodynamic model, the performance of each component of the ammonia–water absorption cycle has been determined. Based on different working conditions, the coefficient of performance (COP), reversible coefficient of performance (COP_E) and exergetic efficiency (η_{ex}) were calculated. The results are presented graphically as a function of varying temperatures for each component of the system.

Imperfect heat and mass transfer in the cycle, mixing losses and circulation losses lead the system to the irreversibilities which reduce COP and exergetic efficiency to a lower value than the ideal reversible cycle in the absorption system. The mixing losses are due to the heat of mixing in the NH_3–H_2O solution.

Table 1 shows the various thermodynamic values in the cycle operation that have been obtained from the analysis at $T_{\text{gen}} = 80$ °C, $T_{\text{con}} = 30$ °C, $T_{\text{abs}} = 30$ °C, $T_{\text{eva}} = 2$ °C and a cooling load of 10 kW with an assumed solution heat exchanger effectiveness of 80%. The results of the first law analysis are presented in Table 2, which illustrates various energy flows to and from each component of the system. The performance parameters and the exergetic efficiency are also shown in this table. The percentage of exergy losses of different components of the system at the same operating conditions are represented in Fig. 3. It is noticed that around 63% of the total exergy loss is taking place in the absorption process. The second worst component from the viewpoint of exergy loss is the generator, followed by the condenser. These irreversibilities are mainly due to heat exchange across a large temperature difference in the absorber and mass transfer with a high concentration gradient and mixing losses in the generator and the absorber [28]. In addition, as the ammonia leaving the generator is superheated, a higher temperature is required under the same pressure, which leads to higher thermodynamic losses in the generator as well as in the absorber. The superheated temperature also drives the extra cooling requirement for the condenser which leads to the exergy losses in the condenser [6].

The coefficient of performance (COP), reversible coefficient of performance (COP_E) and exergetic efficiency (η_{ex}) of this absorption cycle are plotted in Fig. 4 as functions of the generator temperature. The reversible COP_E increases with increasing generator temperature. The coefficient of performance (COP) and the exergetic efficiency pass through maxima at 80 °C and 70 °C respectively. After the maximum point, the gradient of the COP curve becomes almost flat whereas the exergetic efficiency decreases rapidly. This suggests that the exergetic efficiency is more affected by increasing generator temperature than that of the COP. Although the higher generator temperature can produce more ammonia vapor, it also increases the solution temperature in the absorber and the generator which leads to more exergy losses in the absorber and the generator as well as in the condenser. As a result, the total exergy loss of the system is varying with the generator temperature as presented in Fig. 5. The circulation ratio also decreases with an increase in generator temperature as shown in Fig. 6. If the generator temperature approaches its low temperature limit, the circulation ratio increases dramatically. Therefore, it is impractical to operate this cycle when the generator temperature is below

Table 1
Thermodynamic properties at different states in ammonia–water absorption cycle at operating conditions $T_{gen} = 80\ ^{\circ}C$, $T_{con} = 30\ ^{\circ}C$, $T_{abs} = 30\ ^{\circ}C$, $T_{eva} = 2\ ^{\circ}C$, $\eta_{HEx} = 80\%$ and a cooling load of 10 kW.

Point	Temperature (°C)	Pressure (kPa)	Mass flow (kg/s)	% Concentration	Enthalpy (kJ/kg)	Entropy (kJ/kg K)	Exergy, e (kJ/kg)
Generator ref exit (1)	80	1166.92	0.0089	100	1627.00	5.704	28.75
Condenser ref exit (2)	30	1166.92	0.0089	100	340.78	1.455	9.36
Evaporator ref inlet (3)	2	461.67	0.0089	100	340.78	1.536	−14.81
Evaporator ref exit (4)	2	461.67	0.0089	100	1465.82	5.595	−99.94
Absorber sol exit (5)	30	461.67	0.0436	55.05	−114.25	0.609	20.30
Sol HEX inlet (6)	30	1166.92	0.0436	55.05	−114.25	0.609	20.30
Generator sol inlet (7)	62	1166.92	0.0436	55.05	35.42	0.663	153.67
Generator sol exit (8)	80	1166.92	0.0347	43.90	110.85	0.517	272.80
Sol HEX exit (9)	40	1166.92	0.0347	43.90	−77.13	0.459	101.95
Absorber sol inlet (10)	40	461.67	0.0347	43.90	−77.13	0.459	101.95

Table 2
Energy flow for different components in ammonia–water absorption cycle.

Generator, Q_{gen}	16.77 kW
Condenser, Q_{con}	11.43 kW
Evaporator, Q_{eva}	10.00 kW
Absorber, Q_{abs}	15.33 kW
Heat exchanger, Q_{HEx}	6.53 kW
Pump, W_p	0.89 mW
COP	0.60
Reversible, COP_E	1.86
Exergetic efficiency, η_{ex}	32.01%
Circulation ratio, CR	4.91

about 70 °C. So, the negative effect of increasing generator temperature can assist in optimizing the driving temperature of this 10 kW absorption cooling system, which lies between 70 and 80 °C. This temperature range can be achieved by using flat plate solar collectors which are generally appropriate for temperatures below 90 °C [37].

The effects of the evaporator temperature are illustrated in Figs. 7 and 8. With varying the evaporator temperature from −4 to 16 °C; both COP and reversible COP_E increase. The higher evaporator temperature causes a higher absorbing pressure which significantly increases the absorption efficiency of the weak solution. With constant cooling load, the absorber and generator thermal loads decrease with increasing evaporator temperature leading to the COP increases. But the increase of COP is almost linear while that of the reversible COP_E is incremental with increasing evaporator temperature. The impact of other variables of the system causes the actual COP to be almost linear. Unlike COP, increasing the evaporator temperature has a negative impact on the exergetic efficiency. It can be seen that the absorption cooling system has a higher exergetic efficiency at lower evaporator temperatures. This means that the evaporator has a higher potential for cooling at its lower temperature. It is also shown in Fig. 8 that increasing evaporator temperature has very little impact on the total exergy loss of the system as compared to increasing the generator temperature. From the analysis of energy and exergy, it can be explained that the required cooling effect can be achieved by decreasing the evaporator temperature.

The relationship between the COP, reversible COP_E, exergetic efficiency and condenser temperature are shown in Fig. 9. A decrease of the system performance and exergetic efficiency occur with increasing condenser temperature. As the system is considered reversible, meaning that the system is a reversible Carnot heat engine and Carnot refrigerator, so the heat transfer between the condenser and the environment occurs across an infinitesimal temperature difference. The overall maximum thermal performance of an absorption refrigeration system under reversible conditions depends on only the heat from the source (generator) and heat removed from the refrigerated space by the evaporator. As the reversible COP_E depends on the generator and the evaporator temperature, there is no condenser temperature impact on the reversible COP_E. With a constant cooling load, increasing the condenser temperature causes a higher pressure in the system, which increases the thermal load on the generator. This results in less ammonia vapor released from the generator, so both COP and exergetic efficiency decrease. This explains why the maximum system performance and exergetic efficiency are attained at lower values of condenser temperature. It can also be seen from Fig. 10 that the total exergy loss also increases rapidly with increasing condenser temperature. The exergy loss in the condenser results from the temperature difference between the environment and the

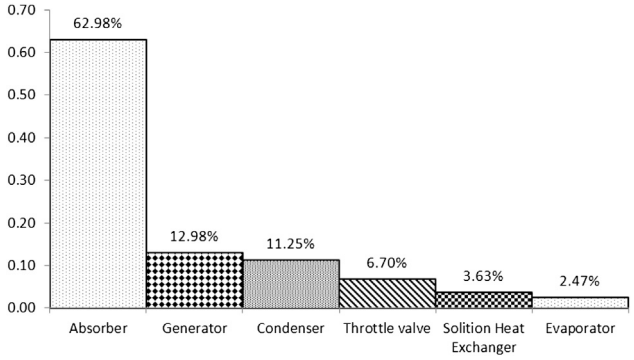

Fig. 3. Non-dimensional exergy loss of different components of a 10 kW system at $T_{gen} = 80\ ^{\circ}C$, $T_{con} = 30\ ^{\circ}C$, $T_{abs} = 30\ ^{\circ}C$, $T_{eva} = 2\ ^{\circ}C$, $\eta_{HEx} = 80\%$.

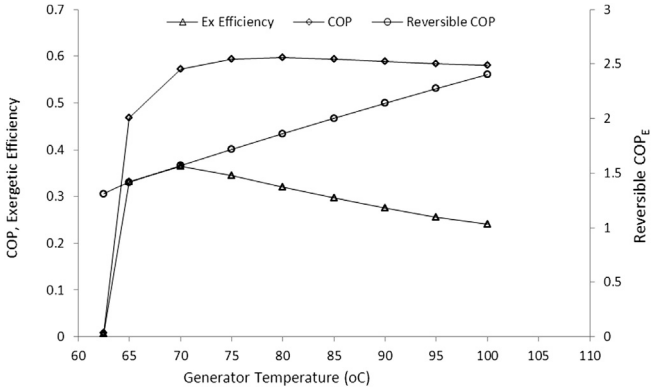

Fig. 4. Effect of generator temperature on the COP, reversible COP_E and exergetic efficiency at $T_{con} = 30\ ^{\circ}C$, $T_{abs} = 30\ ^{\circ}C$, $T_{eva} = 2\ ^{\circ}C$, $\eta_{HEx} = 80\%$.

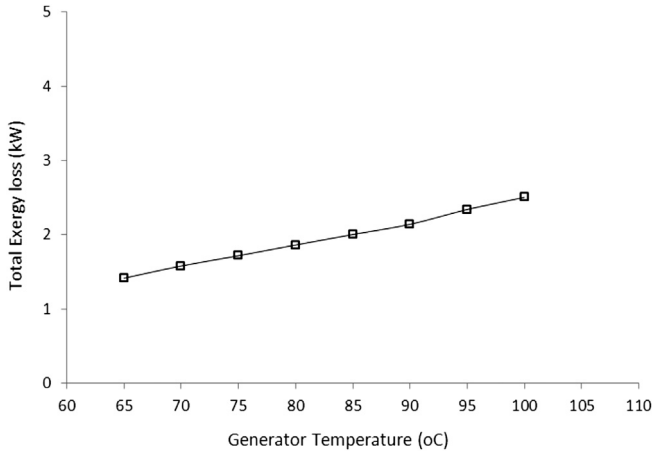

Fig. 5. Effect of generator temperature on the total exergy loss of the system at $T_{con} = 30\ ^{\circ}C$, $T_{abs} = 30\ ^{\circ}C$, $T_{eva} = 2\ ^{\circ}C$, $\eta_{HEx} = 80\%$.

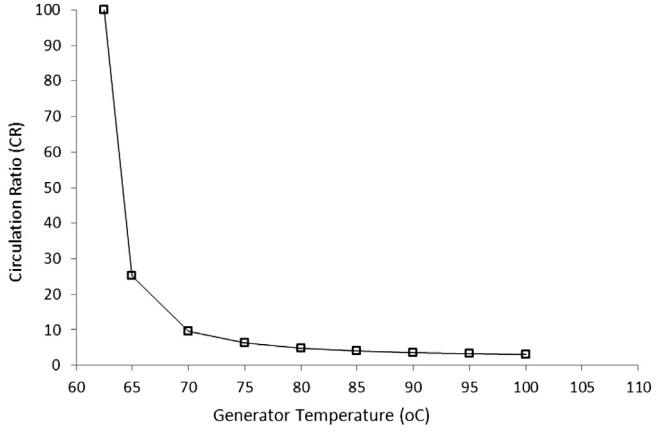

Fig. 6. Effect of generator temperature on the circulation ratio (CR) at $T_{con} = 30\ ^{\circ}C$, $T_{abs} = 30\ ^{\circ}C$, $T_{eva} = 2\ ^{\circ}C$, $\eta_{HEx} = 80\%$.

condenser refrigerant. So the exergy and the system performance benefit from lower condenser temperatures.

The result of the absorber temperature's effect is the same as that of the condenser temperature for both the system performance as well as for the exergy loss. Fig. 11 shows the variation of

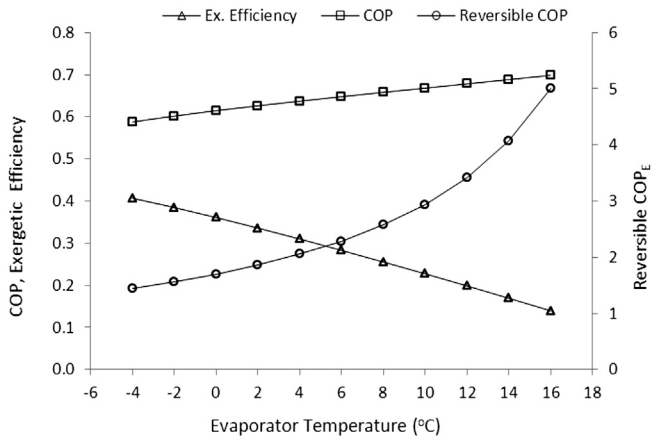

Fig. 7. Effect of evaporator temperature on the COP, reversible COP_E and exergetic efficiency of 10 kW system at $T_{gen} = 80\ ^{\circ}C$, $T_{con} = 30\ ^{\circ}C$, $T_{abs} = 30\ ^{\circ}C$, $\eta_{HEx} = 80\%$.

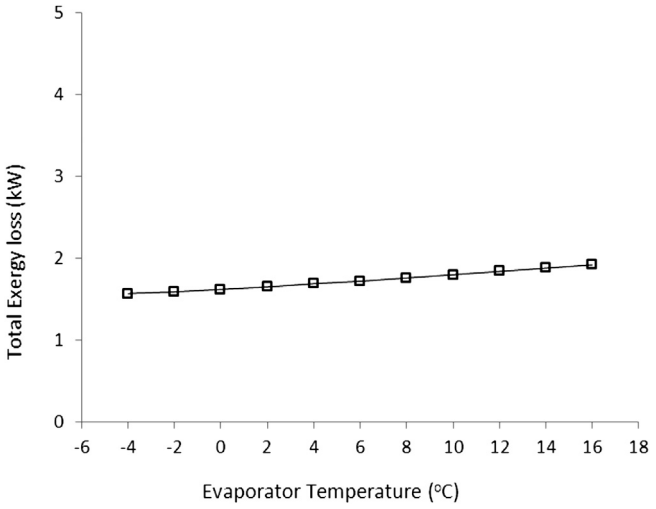

Fig. 8. Effect of evaporator temperature on the total exergy loss of 10 kW system at $T_{gen} = 80\ ^{\circ}C$, $T_{con} = 30\ ^{\circ}C$, $T_{abs} = 30\ ^{\circ}C$, $\eta_{HEx} = 80\%$.

the COP, reversible COP_E and exergetic efficiency with the absorber temperature. Increasing absorber temperature decreases the absorption efficiency of the weak solution in the absorber. As a result, with a constant cooling load, absorber and generator thermal loads increase, therefore the COP decreases. The reversible COP_E remains constant as was the case for varying condenser temperature. The higher system performance can be achieved at lower absorber temperature. The increasing absorber temperature increases the solution temperature in the absorber as well as in the generator which leads to greater mixing losses in the absorber and the generator. The increasing solution temperature also affects the heat exchanger. As a result, high temperature solution is entering the absorber. These increase the exergy loss of the heat exchanger as well as of the absorber. This leads to a significant increase in the total exergy loss of the system. Fig. 12 illustrates the corresponding effect of the system exergy loss versus absorber temperature.

Energy and exergy analyses of each component of this small cooling absorption system determine the optimum operation conditions for the best system performance. It also reveals that the absorber, the generator, and the condenser represent the most of

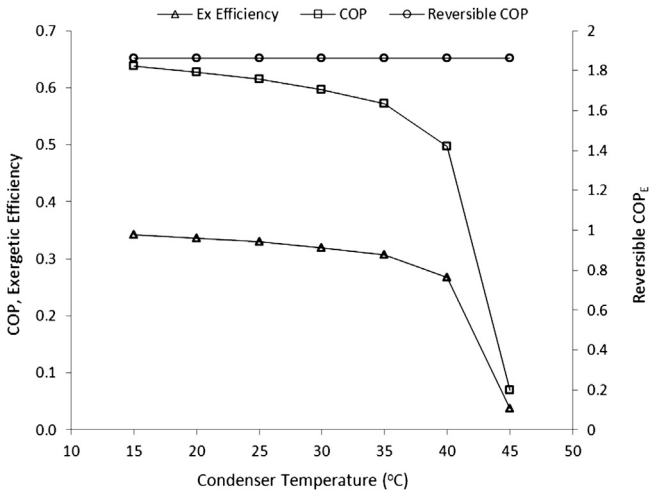

Fig. 9. Effect of condenser temperature on the COP, reversible COP_E and exergetic efficiency of 10 kW system at $T_{gen} = 80\ ^{\circ}C$, $T_{abs} = 30\ ^{\circ}C$, $T_{eva} = 2\ ^{\circ}C$, $\eta_{HEx} = 80\%$.

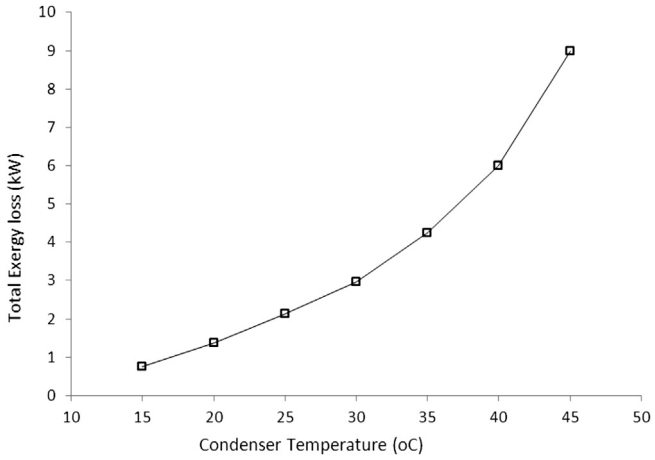

Fig. 10. Effect of condenser temperature on the total exergy loss of 10 kW system at $T_{gen} = 80\ ^{\circ}C$, $T_{abs} = 30\ ^{\circ}C$, $T_{eva} = 2\ ^{\circ}C$, $\eta_{HEx} = 80\%$.

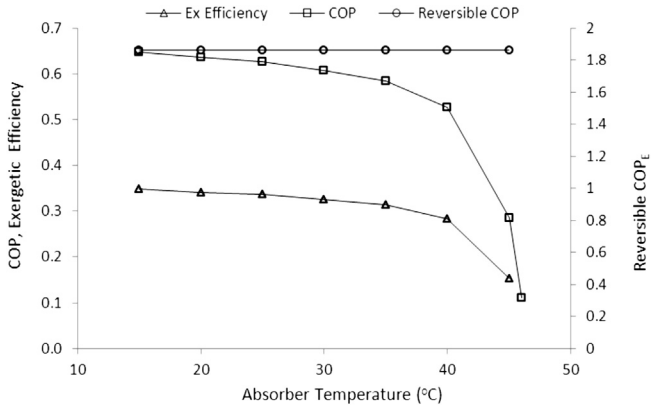

Fig. 11. Effect of absorber temperature on the COP, reversible COP_E and exergetic efficiency of 10 kW system at $T_{gen} = 80\ ^{\circ}C$, $T_{con} = 30\ ^{\circ}C$, $T_{eva} = 2\ ^{\circ}C$, $\eta_{HEx} = 80\%$.

the total exergy losses of the chiller. For an ideal process, the reversible COP_E is 1.86. The potential degradation of all components results in an actual COP of 0.60. The absorber has the greatest potential to improve the system performance. This component needs the maximum design improvement following by the generator and the condenser in order to reduce their exergy loss rate resulting of reducing the irreversibility.

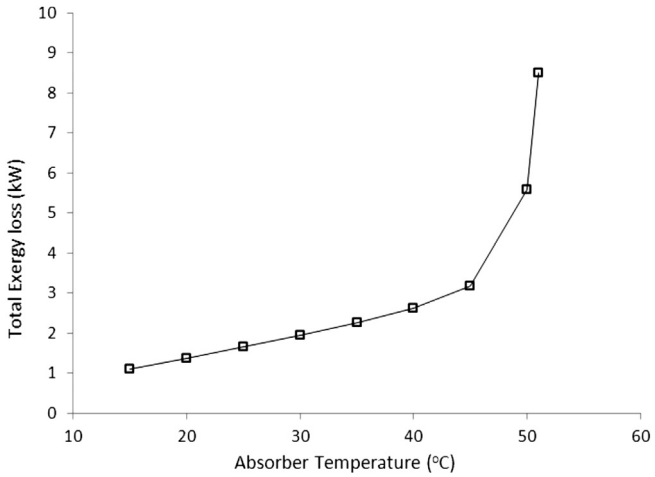

Fig. 12. Effect of absorber temperature on the total exergy loss of 10 kW system at $T_{gen} = 80\ ^{\circ}C$, $T_{con} = 30\ ^{\circ}C$, $T_{eva} = 2\ ^{\circ}C$, $\eta_{HEx} = 80\%$.

5. Conclusions

The goal of this study was to maximize the efficiency of an absorption chiller that can be used for residential air conditioning application with a low temperature driving source such as solar thermal energy. In this regard, energy and exergy analyses of a 10 kW air-cooled ammonia–water absorption chiller have been performed and the system performance, exergetic efficiency and the exergy loss of different components of the system have been calculated.

The first and second law efficiency of the system have been investigated and compared under different system operating conditions. The results show that the COP of the system increases slightly with increasing heat source temperature and the evaporator temperature but decreases as absorber and condenser temperatures increase. However, the exergetic efficiency decreases with the increase of generator, evaporator, condenser and absorber temperatures. The analysis reveals that the cycle is more thermodynamically efficient when the absorption cooling system is operated using low temperature heat sources rather than high temperature heat sources and it has also been noticed that decreasing of the condenser and the absorber temperatures towards the atmospheric temperature does not impact significantly the overall system performance. So, for small scale applications, an ammonia–water absorption chiller can be operated with heat supplied by a flat plate solar collector with ambient air cooling of the absorber and the condenser.

The exergy analysis of this absorption cooling system shows that the highest exergy loss (around 76%) is located in the absorbing process and in the generator. In order to improve cycle efficiency, the highest efforts should be given to improving the absorber while the generator may be considered as the second priority.

Finally, the energy and exergy analyses in this paper offer a simple and effective method to identify where losses are taking place in the small ammonia–water absorption cooling system and how these affect the system performance. It also offers insight into which component should be modified in design for the best performance of the system. Additionally, the results can also be used in thermoeconomic optimization of absorption systems. The thermoeconomic optimization of the system can take into account "the costs and benefits (or "profitability") of the various mechanisms for utilizing and capturing available energy to do work" [11].

Acknowledgements

This work is made possible by the Natural Science and Engineering Research Council of Canada.

Nomenclature

COP	coefficient of performance
COP_E	coefficient of performance under reversible condition
CR	circulation ratio
e	specific exergy (kJ/kg)
E_D	exergy destruction or loss (kW)
h	specific enthalpy (kJ/kg)
h_o	specific enthalpy at reference temperature 25 °C
HEX	heat exchanger
H_2O	water
GAX	generator–absorber exchanger
kW	kilowatt

$\dot{m}$	mass flow rate (kg/s)
NH_3	ammonia
P	pressure (kPa)
P_o	reference pressure 101.325 kPa
$\dot{Q}$	heat transfer rate (kW)
ref	refrigerant
s	specific entropy (kJ/kg K)
s_o	specific entropy at reference temperature 25 °C
sol	solution
T	temperature (K)
T_o	reference temperature 25 °C
X	mass fraction of ammonia (%)
$\dot{W}$	work rate (kW)
η_{HEx}	heat exchanger efficiency
η_{ex}	exergetic efficiency
v	pump specific volume (m^3/kg)

Subscripts

abs	absorber
con	condenser
eva	evaporator
gen	generator
i	component
in	inlet
out	outlet
p	pump

References

[1] J.M. Abdulateef, K. Sopian, M.A. Alghoul, Optimum design for solar absorption refrigeration systems and comparison of the performances using ammonia–water, ammonia–lithium nitrate and ammonia–sodium thiocyanate solutions, Int. J. Mech. Mater. Eng. (IJMME) 3 (2008) 17–24.

[2] S.A. Adewusi, S.M. Zubair, Second law based thermodynamic analysis of ammonia–water absorption systems, Energy Convers. Manage. 45 (2004) 2355–2369.

[3] G.S. Alamdari, Simple equations for predicting entropy of ammonia–water mixture, Int. J. Eng. (IJE) Trans. B: Appl. 20 (2007) 97.

[4] S. Aphornratana, I.W. Eames, Thermodynamic analysis of absorption refrigeration cycles using the second law of thermodynamics method, Int. J. Refrig. 18 (1995) 244–252.

[5] M.S.S. Ashhab, H. Kaylani, A. Abdallah, PV solar system feasibility study, Energy Convers. Manage. 65 (2013) 777–782.

[6] M. Barhoumi, N.B. Ezzine, A. Bellagi, Exergy analysis of an ammonia–water absorption system, Int. J. Exergy 6 (5) (2009).

[7] F. Boudéhenn, H. Demasles, J. Wyttenbach, X. Jobard, D. Chèze, P. Papillon, Development of a 5 kW cooling capacity ammonia–water absorption chiller for solar cooling applications, Energy Procedia 30 (2012) 35–43.

[8] Y. Cengel, M. Boles, Thermodynamics: an Engineering Approach, McGraw-Hill, 2008.

[9] Central Electricity Authority (CEA), Ministry of Power, Government of India, June 2013.

[10] B. Choudhury, P.K. Chatterjee, J.P. Sarkar, Review paper on solar-powered air-conditioning through adsorption route, Renew. Sustain. Energy Rev. 14 (2010) 2189–2195.

[11] P.A. Corning, Thermoeconomics: beyond the second law, J. Bioecon. 4 (2002) 57–88.

[12] A. De Francisco, R. Illanes, J.L. Torres, M. Castillo, M. De Blas, E. Prieto, A. Garcia, Development and testing of a prototype of low-power water–ammonia absorption equipment for solar energy applications, Renew. Energy 25 (2002) 537–544.

[13] J. Deng, R.Z. Wang, G.Y. Han, A review of thermally activated cooling technologies for combined cooling, heating and power systems, Prog. Energy Combust. Sci. 37 (2011) 172–203.

[14] S. Du, R.Z. Wang, P. Lin, Z.Z. Xu, Q.W. Pan, S.C. Xu, Experimental studies on an air-cooled two-stage NH_3–H_2O solar absorption air-conditioning prototype, Energy 45 (2012) 581–587.

[15] N. Ezzine, B. Barhoumi, M. Mejbri, K. Chemkhi, S.A. Bellagi, Solar cooling with the absorption principle: first and second law analysis of an ammonia–water double-generator absorption chiller, desalination Strategies in South Mediterranean countries, Desalination 168 (2004) 137–144.

[16] K.F. Fong, T.T. Chow, C.K. Lee, Z. Lin, L.S. Chan, Comparative study of different solar cooling systems for buildings in subtropical city, Solar Energy 84 (2010) 227–244.

[17] R. Gomri, Investigation of the potential of application of single effect and multiple effect absorption cooling systems, Energy Convers. Manage. 51 (2010) 1629–1636.

[18] M. Hammad, S. Habali, Design and performance study of a solar energy powered vaccine cabinet, Appl. Therm. Eng. 20 (2000) 1785–1798.

[19] M. Henning, Solar assisted air conditioning of buildings – an overview, Appl. Therm. Eng. 27 (2007) 1734–1749.

[20] H.Z. Hassan, A solar powered adsorption freezer: a case study for Egypt's Climate, Int. J. Energy Eng. 3 (2013) 21–29.

[21] A. Häberle, F. Luginsland, C. Zahler, M. Berger, M. Rommel, H.M. Henning, et al., A linear concentrating Fresnel collector driving a NH_3–H_2O absorption chiller, in: Proceedings of the Second International Conference Solar Air-Conditioning, Tarragona, Spain, 2007, pp. 662–667.

[22] IPCC, Intergovernmental Panel on Climate Change. IPCC Fourth Assessment Report: Climate Change, 2007.

[23] M. Izquierdo, M. Venegas, P. Rodríguez, A. Lecuona, Crystallization as a limit to develop solar air-cooled LiBreH2O absorption systems using low-grade heat, Sol. Energy Mater. Sol. Cells 81 (2004) 205–216.

[24] U. Jakob, U. Eicker, Solar cooling with diffusion absorption principle, in: World Renewable Energy Congress VII, Cologne, Germany, 29 June–5 July, 2002.

[25] U. Jakob, W. Pink, Development and investigation of an ammonia/water absorption chiller – chillii_ PSC – for a solar cooling system, in: Proceedings of the 2nd International Conference Solar Air-conditioning, Tarragona, Spain, 2007, pp. 440–445.

[26] U. Jakob, K. Spiegel, W. Pink, Development and experimental investigation of a novel 10 kW ammonia/water absorption chiller for air conditioning and refrigeration systems, in: 9th International IEA Heat Pump Conference, Zürich, Switzerland, 20–22 May, 2008.

[27] N. Kalkan, E.A. Young, A. Celiktas, Solar thermal air conditioning technology reducing the footprint of solar thermal air conditioning, Renew. Sustain. Energy Rev. 16 (2012) 6352–6383.

[28] S.E.I. May, I. Boukholda, A. Bellagi, Energetic and exergetic analysis of a commercial ammonia–water absorption chiller, Int. J. Exergy 8 (1) (2011).

[29] OECD/IEA, Technology Roadmap Solar Heating and Cooling, International Energy Agency, 2012.

[30] S. Raghuvansh, G. Maheshwari, Analysis of ammonia–water (NH_3–H_2O) vapor absorption refrigeration system based on first law of thermodynamics, Int. J. Sci. Eng. Res. 2 (2011) 2229–5518.

[31] W. Ryan, New developments in gas cooling, ASHRAE J. 4 (2002) 23–26.

[32] V. Sabatelli, G. Fiorenza, D. Marano, Technical Status Report on Solar Desalination and Solar Cooling. A technical report of the EU-project "NEGST (New Generation of Thermal Solar Systems)" WP5.D1, 2007, http://www.swt-technologie.de/html/publicdeliverables3.html.

[33] A. Sencan, K.A. Yakuta, S.A. Kalogirou, Exergy analysis of lithium bromide/water absorption systems, Renew. Energy (2005) 645–657.

[34] A.I. Shahata, M.M. Aboelazm, A.F. Elsafty, Energy and exergy analysis for single and parallel flow double effect water-lithium bromide vapor absorption systems, Int. J. Sci. Technol. 2 (2012) 85–94.

[35] A. Sozen, D. Altiparmak, H. Usta, Development and testing of a prototype of absorption heat pump operated by solar energy, Appl. Therm. Eng. 22 (2002) 1847–1859.

[36] D.W. Sun, Comparison of the performances of NH_3–H_2O, NH_3–$LiNO_3$ and NH_3–NaSCN absorption refrigeration systems, Energy Convers. Manage. 39 (1998) 357–368.

[37] M. Treberspurg, M. Djalili, H. Staller, New Technical Solutions for Energy Efficient Buildings. State of the Art Report: Solar Heating & Cooling, SCI-Network: Sustainable Construction & Innovation Through Procurement, July 2011.

[38] R. Vidal, R. Best, R. Rivero, J. Cerventas, Analysis of a combined power and refrigeration cycle by the exergy method, Energy 31 (2006) 3401–3414.

[39] R.Z. Wang, T.S. Ge, C.J. Chen, Q. Ma, Z.Q. Xiong, Solar sorption cooling systems for residential applications: options and guidelines, Int. J. Refrig. 32 (2009) 638–660.

[40] L. Zhu, J. Gu, Second law-based thermodynamic analysis of ammonia/sodium thiocyanate absorption system, Renew. Energy 35 (2010) 1940–1946.